Supporting information for:

# Low temperature epitaxy of tungsten-telluride heterostructure films

P.A. Vermeulen, J. Momand, B.J. Kooi

Zernike institute for Advanced Materials, University of Groningen.
Nijenborgh 4, 97647 AG Groningen, The Netherlands.
Corresponding Author: B.J.Kooi@rug.nl

SI-1. Target ablation track analysis

The single crystal (SC) and sintered powder (SP) targets of $WTe_2$ were investigated after several depositions using energy dispersive X-ray spectroscopy (EDS) attached to SEM. EDS was performed within and outside the ablation track for direct comparison. The results are shown in table 1.

The EDS scans show that the ablated track is still close to stoichiometric $WTe_2$, albeit with some slight Te-deficiency. The trend is consistent for both SC and SP targets. Figure 1 shows a composition-sensitive Back-Scattered Electron (BSE) image of the ablation track on the SC target. The track looks relatively smooth and no phase segregation is observed. Outside the ablation track globules of redeposited Te are observed, which indicates that slight post-pulse Te evaporation (and redeposition) takes place. This process reduces the Te content within the ablated area over time. The Te evaporation effect seems comparable for both powder and single-crystal targets. We conclude that the $WTe_2$ targets *ablate* stoichiometrically (at a fluence of 1 $Jcm^2$). Targets needs to be grazed periodically however, to avoid worsening the evaporation effect over time.

| At.% Te | Powder | Single Crystal |
|---|---|---|
| Pristine | 64.8 | 66.0 |
| Ablated | 60.8 | 61.5 |

*Table 1. SEM-EDS analysis of the powder- and single-crystal targets, at.% Te measured on a pristine area and an ablated area. The measurement error is on the order of a few at.%.*

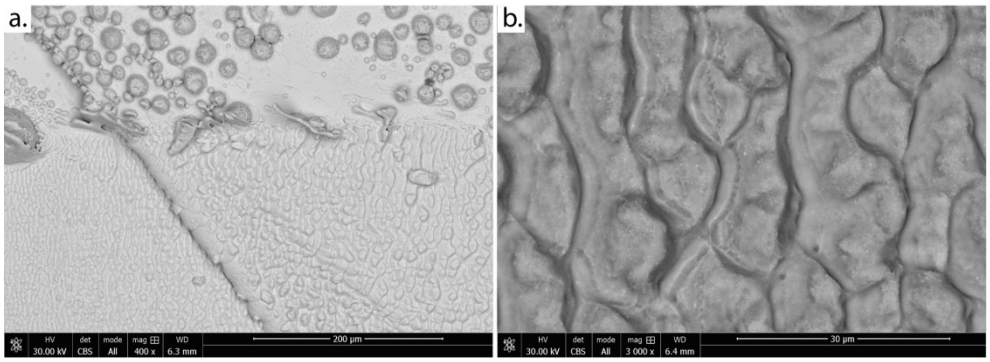


*Figure S1. a.) Back-Scattered Electron (BSE) scan of the SC $WTe_2$ target. The ablation track on the bottom shows uniform small features, the darker globular structures outside the ablation track consist of redeposited Te. The diagonal line is a crystalline step edge which is preserved across many depositions. b.) Higher magnification BSE scan of the deposition track. The contrast is formed due to roughness, the scan shows no phase segregation.*

After a few depositions the targets show some roughness. When it is not grazed, this roughness is exacerbated on each subsequent distribution, creating an often-seen pillar structure, where one element is preferentially evaporated, in this case the tellurium. The effects can be clearly seen in figure S2.

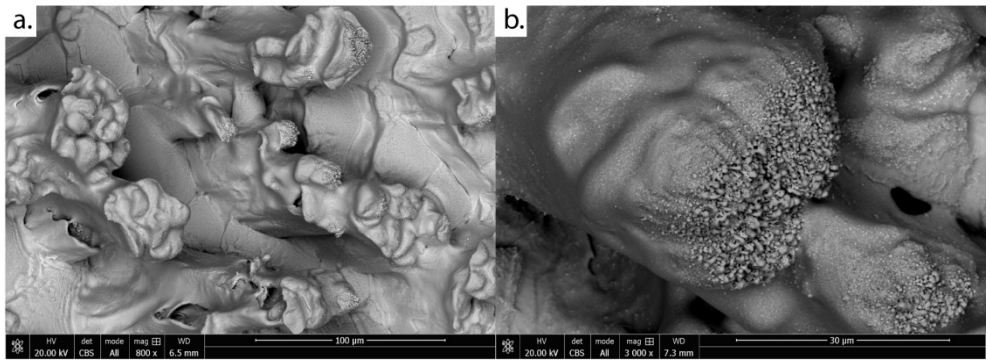


*Figure S2. a.) Single-crystal target after extended ablation without grazing. b.)The pillar shows extensive W-enrichment: the white features are pure W.*

SI-2. Influence of process gas on the $WTe_2$ deposition.

A $WTe_2$ deposition was performed at higher chamber pressure than normal, using a fluence of 0.8 Jcm² at room temperature. The results are shown in table S2. The Te content dropped by 20 at.%, which we speculate is due to the lower mass of Te allowing it to be scattered by the process gas more easily than W.

| Ar Pressure (mBar) | At.% Te |
|---|---|
| $10^{-2}$ | 57 |
| $10^{-7}$ | 78 |

*Table S2. Atomic concentration Te for high and low process pressure. Te is preferentially stopped from reaching the substrate.*

SI-3. Fluence and temperature tuning on amorphous carbon TEM-grids

A typical bright-field view of a $WTe_2$ film on amorphous carbon is shown in figure S3. The films are typically homogeneous and smooth, except for small crystalline W droplets. The films are amorphous, unless one grows on a broken and wrinkled carbon grid. Then the film crystallizes in a circular area around the hole, presumably due to the higher availability of nucleation sites.

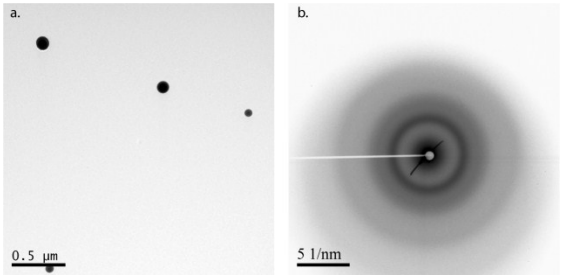


*Figure S3. a.) An amorphous $WTe_2$ film as deposited on carbon film. b.) SAED of the area shown in a. The broad rings indicate an amorphous or nanocrystalline film.*

SI-4. Use of Mica-$Bi_2Te_3$ seed crystal.

Two $WTe_2$ films were grown using a mica substrate and single-crystal target. For one film, a seed layer $Bi_2Te_3$ was deposited first. For this seed, the deposition temperature was 210 °C, fluence was 1 $Jcm^{-2}$, gas pressure 0.12 mBar Argon. The RHEED in figure S4 shows that the $WTe_2$ film is amorphous or highly disordered without this seed layer. Figure S5 shows sharp interfaces with both mica and $WTe_2$ are formed by the $Bi_2Te_3$.

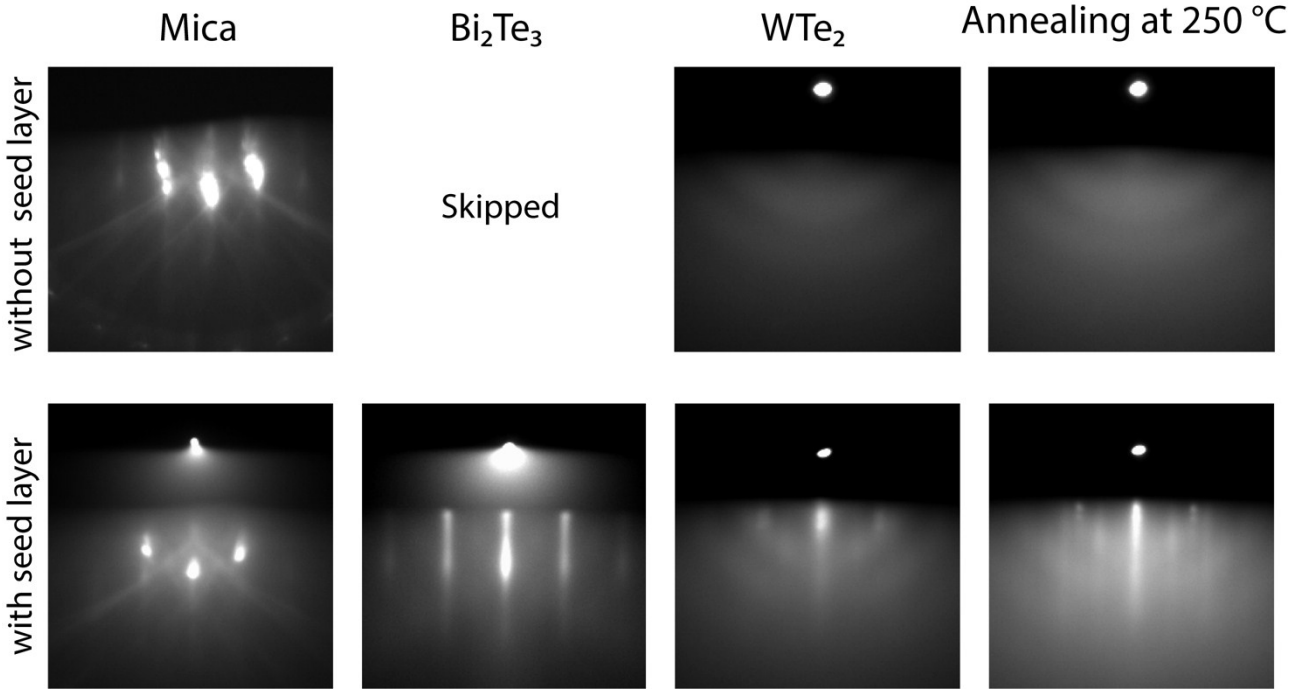


*Figure S4. RHEED patterns of substrate (mica), seed crystal ($Bi_2Te_3$) and $WTe_2$ layer. It shows the use of a seed crystal is essential for obtaining an ordered $WTe_2$ film. Furthermore, when $Bi_2Te_3$ is used the figure shows epitaxial alignment of all sublayers.*

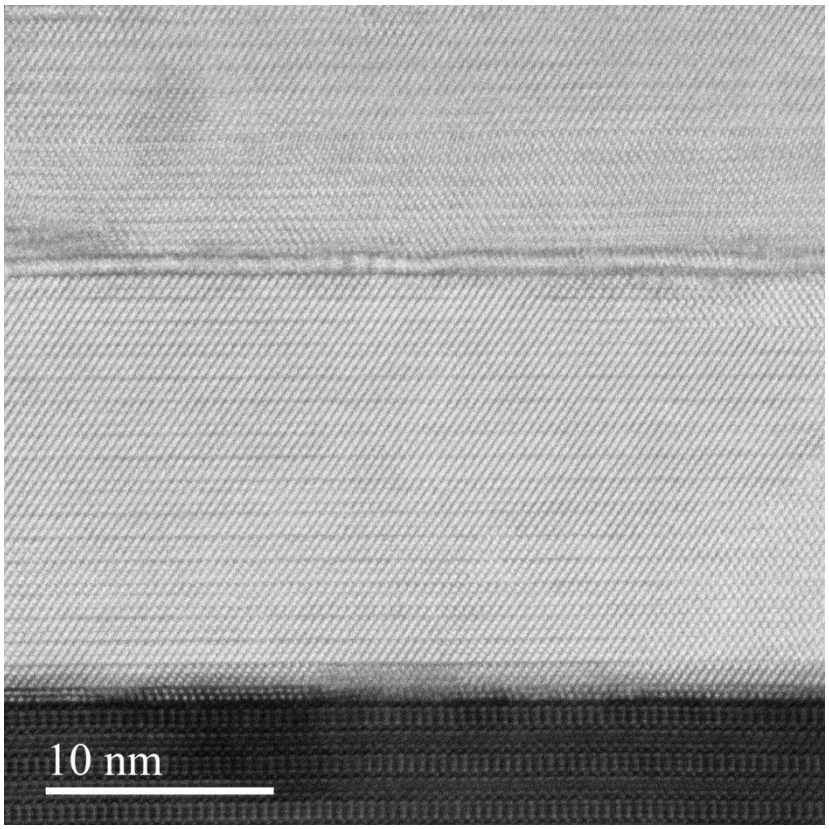


*Figure S5. HAADF-STEM image showing the muscovite mica substrate, $Bi_2Te_3$ seed crystal, and one monolayer of $WTe_2$. Another block of $Bi_2Te_3$ was grown on top. The individual layers have grown fully epitaxially, and the vdWaals gaps are clearly resolved in all materials.*

SI-5. EDS Analysis of the bilayer on SiO2 window

EDs analysis was performed on a bilayer of $Bi_2Te_3$ and $WTe_2$. To obtain the atomic composition of this film, the background from the TEM instrument and substrate (Si, C, Cu, O) was removed from the total composition. Two measurements on different film areas were performed. Due to the extremely low thickness, the film signal intensity is quite low. Nevertheless, both measurements closely agree. The normalized intensity is calculated, as well as the nominal composition of this $WTe_2$-$Bi_2Te_3$ bilayer system.

| At.% | Area 1 | Area 2 | stdev | avg | Normalized 100% | Normalized & Stoichiometric |
|---|---|---|---|---|---|---|
| Te | 11.31 | 10.21 | 0.78 | 10.76 | 60.42 | 64.00 |
| W | 4.10 | 3.74 | 0.26 | 3.92 | 22.00 | 20.01 |
| Bi | 3.25 | 3.01 | 0.18 | 3.13 | 17.58 | 15.99 |

*Table S2. Atomic content of the bilayer constituent species. The composition is measured in two distinct areas. Both scans show similar composition within the fitting area of the EDS algorithm. The average normalized compositions are calculated, as well as the stoichiometric composition closest to the observed composition.*